Research Article

Experimental investigation of gas-brine liquid flow in horizontal pipeline

Norhafizuddin Husein[1] · Issham Ismail[1] · Sanjihuen V. Selva Mani[1] · Wong Zhu Ker[1] · Natalie Vanessa Boyou[1,2] · Ahmad Shamsul Izwan Ismail[1,3] · Wan Rosli Wan Sulaiman[1]

Received: 17 August 2020 / Accepted: 23 November 2020 / Published online: 12 December 2020

Abstract
Pipelines that are transporting fluids of different salinity in different pressurized conditions are met with different behaviors of flow. Flow behavior of two-phase gas–liquid system in simulated horizontal pipeline conditions are investigated experimentally with three different brine salinity concentrations comparable to the reservoir fluid properties within the Malay Basin. A test facility in total length of 80-feet was designed and configured for data acquiring of flow regimes which were observed via a 1.5-in diameter and a 7.5-feet long transparent acrylic pipe. A flow regime map where the transition of flow pattern from stratified to intermittent to mixed is proposed as the superficial gas velocity and superficial liquid velocity increase at increasing brine concentration. There is a combination flow pattern presumed to be the combination of plug flow, slug flow and thin annular. When the brine salinity increases, the pressure drop of the system increases. The lowest pressure drop in the form of percentage for brine concentration of 1000, 15,000, and 30,000 ppm at brine superficial velocity of 3.0 m/s were 57.1, 50, and 42.9% respectively. Pressure drop experimental results from this study were compared with previous mathematical correlations. Results also indicate that water holdup increases when water input fraction increases.

✉ Issham Ismail, issham@petroleum.com.my | [1]Department of Petroleum Engineering, School of Chemical and Energy Engineering, Universiti Teknologi Malaysia, 81310 Johor Bahru, Johor, Malaysia. [2]Department of Petroleum Engineering, School of Engineering, King's College, Aberdeen AB24 3FX, UK. [3]Department of Petroleum Engineering, Asia Pacific University of Technology and Innovation, 57000 Kuala Lumpur, Malaysia.

SN Applied Sciences (2020) 2:2184 | https://doi.org/10.1007/s42452-020-03944-z

Graphic abstract

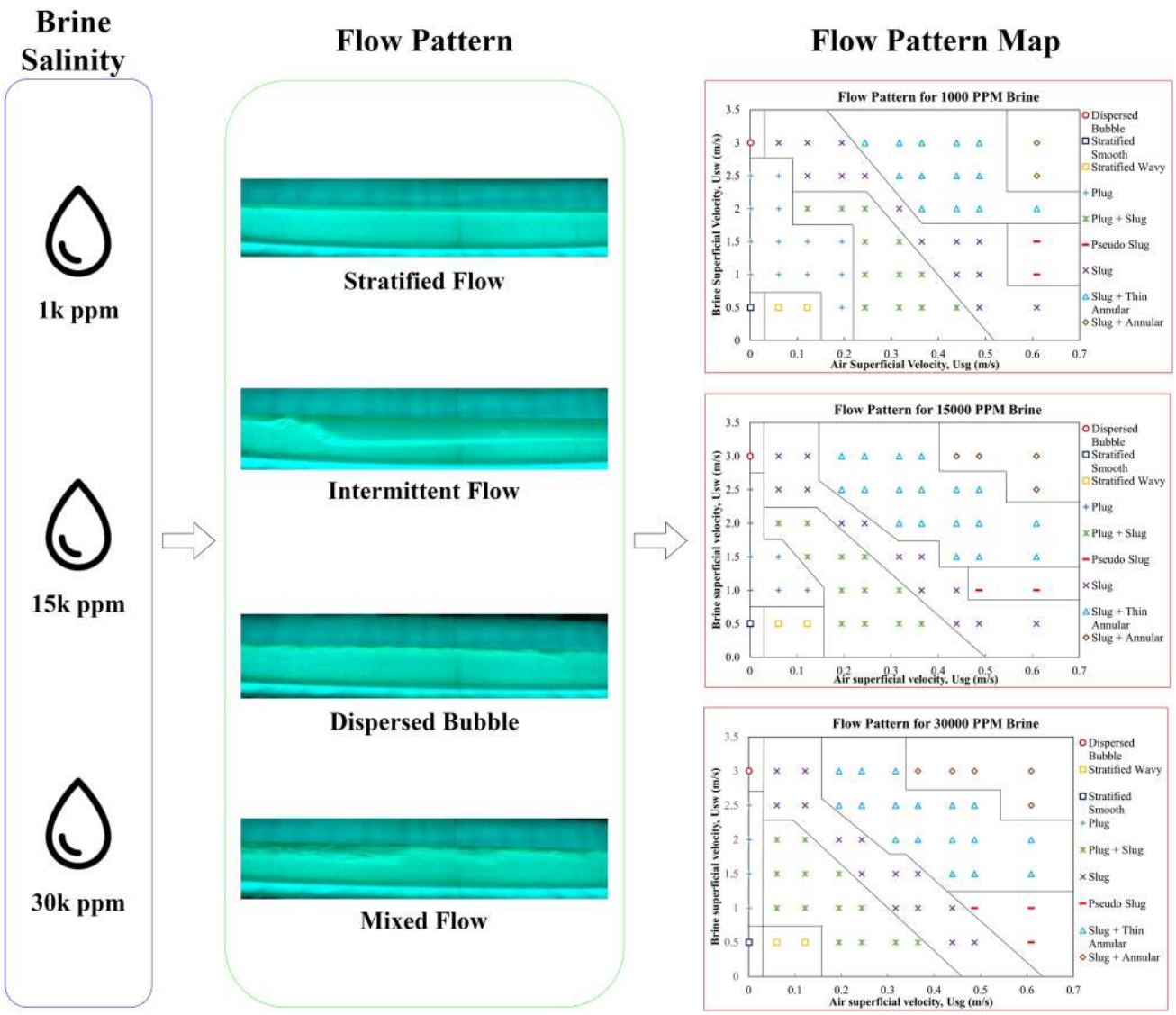

Keywords Two-phase flow · Flow assurance · Flow pattern · Pressure drop · Liquid holdup

1 Introduction

Two-phase gas–liquid flow is ubiquitous in many industries including petroleum, chemical and nuclear industrial applications [1–3]. The understanding of flow pattern in two-phase flow is significant because it is frequently present in chemical processing and in various pipelines in many industries. Flow pattern influences pressure drop and liquid holdup of the gas–liquid system. Pressure drop occurs due to viscous effects along the length of the system, as well as additional pressure losses arising from other technological and piping equipment like valves, elbows, piping entrances, fittings, and tees. In contrast to single-phase pressure drops, calculation and prediction of two-phase pressure drops are much more sophisticated and leading methods differ significantly. Experimental data indicates that the frictional pressure drop in two-phase flow is substantially higher than that for a single-phase flow with the same length and mass flow rate [4]. Liquid holdup, H_w or in situ water fraction is the volume of liquid available in the measured pipe from the total brine and air mixture. The factors affecting H_w are pressure drop,

superficial velocity of liquid and air, the pipe frictional factor, viscosity, and density [5]. In petroleum industry, the most common two-phase flow occurrence is in hydrocarbon transporting pipeline systems and in oil and gas wells. Two-phase flow studies enable us to improve the understanding of flow pattern as well as the behavior of the gas–liquid flow in pipes.

Recent and reliable studies on multiphase flow in petroleum and chemical industries applications has embarked an extensive research effort especially for gas–liquid flow. This is because the varying amount of liquid produced in gas wells affect the production operation performance [6]. The volume, property, and flow rate of the fluid needs to be studied and analyzed in order to efficiently increase the productivity. On the other hand, as of January 1, 2019, Malaysia's estimated natural gas reserves is 97.413 TSCF. The produced natural gas which is processed at PETRONAS Gas Berhad's (PGB) processing plants has been found to contain high CO2 and formation water [7–9]. This indicates that, it is important to conduct a detailed and extensive study on two-phase gas–liquid flow from offshore surface facilities.

It is challenging to determine the production of a gas field when there is a presence of water in the production line. The combination of water and gasses such as CO_2 and H_2S especially at low temperature causes crystalline solid called hydrates to form [10, 11]. According to Armenta and Wojtanowicz [12], water production problem only arises mostly at recovery factor of 30%. The water with various level of salinity depending on the type of reservoir that flows into the well during gas production could lead to various problems and if left undetected could lead to higher non-productive time. The most common problem is corrosion and formation of hydrates. Corrosion causes leakage in casings, tubings and packers, while hydrates cause pipe blockage which in turn restrict production or even a complete shutdown of production, where in some situation can cause rupture to pipeline [13]. This might also cause channeling of water behind the casing that is due to poor cementing which prevents contact of water zone and pay zone [14]. Thus, it is imperative to fully understand the effect of salinity towards flow pattern, pressure drop, and liquid holdup of two-phase air-brine flow in pipelines. Precise measurements of the parameters are crucial in the evaluation for the two-phase flow model [15].

There were multiple studies carried out to understand two-phase gas–liquid flow in the past which included Kong and Kim [2], Mandhane et al, [16], Chen et al, [17], Kumar et al, [18], and Ban et al. [19]. One of the earlier studies was conducted by Mandhane et al. [16] where they compared their flow patterns, particularly in gas–liquid systems with data from University of Calgary Multiphase Pipe Flow data library. They developed an extension of correlation presented by Govier and Aziz [20]. Kong and Kim [2] conducted a characterization study of gas–liquid (water) system in a 1.5-inch experimental flow loop rig with a length of 31.17-feet. The flow loop was equipped with a high-speed video camera to record flow patterns. As a result, they found new transition boundaries and discussed the factors affecting them. In addition, Kumar et al. [18] established a flow pattern map for gas–liquid (water) system in a 0.94-inch acrylic pipe with a length of 26.2-feet. This study focusses solely on flow patterns and they managed to map the flow patterns based on the captured images recorded by a high-speed camera. Furthermore, the researchers noted that the usage of high-speed camera is vital in capturing the transitions of flow patterns. Ban et al. [19] conducted a simulation study of gas-oil flow patterns in a horizontal pipe. Their study focused on the effects of pressure drop, liquid holdup and slug frequency towards slug formation where the model was validated with Baker's flow regime chart. Their findings produced a simplified correlation for liquid holdup and slug frequency. A comparison study focusing on pressure drop in gas–liquid system in small horizontal tubes was conducted by Chen et al. [17] using water and R-401A as the liquid medium. Copper tubing in various inner diameters ranging from 0.04 to 0.2-inch and a fixed length of 2.3-feet is utilized in the research. From the study, the researchers compared their findings with previous correlations and found that The Chisholm and The Friedel correlation are not fit to predict the pressure drop data in small tubes. In short, while myriad studies have been conducted, none of these studies precisely include the effects of salinity towards the flow pattern map, pressure drop, and liquid holdup in horizontal pipelines. There is also scarce literature investigating the effects of salinity and comparing experimental data with previous developed correlation models.

According to Kabiri-Samani et al. [21], there are many parameters and forces affecting two-phase flow in a pipe. However, turbulent diffusivity and buoyant force play the most significant role among others. These are some of the other factors affecting flow behavior. They stated that pressure inside the pipe are a function of:

$$P = \xi\left(Q_a, V_w, D, g, \mu_a, \mu_w, \rho_a, \rho_w, \sigma, \tau_0, f, \varphi\right)$$

where P stands for pressure, Q_a is air discharge, V_w is liquid velocity, D is inner diameter of pipe, g is gravity acceleration, μ_a is air viscosity, μ_w is liquid velocity, ρ_a is air density, ρ_w is liquid density, σ is surface tension, τ_0 is shear stress, f is wave frequency, and φ is inclination angle. In this study, all factors affecting the change in pressure inside the pipe were accounted for except surface tension and wave frequency. Surface tension is not included in this

study because the temperature was kept constant and the amount of sodium chloride added to liquid did not show any significant increase, thus it is negligible. Wave frequency was also neglected as the length of the experimental set up was long enough with sufficient entrance length for flow development.

To the best of the authors' knowledge, there are no experimental data on the effects of salinity towards flow regime in two-phase gas–liquid system in horizontal pipeline and this is supported by Wu et al. [49]. One of the salinity effects on flow regime study was conducted by Mukhaimer et al. [22] but focused on liquid–liquid system (water and oil). The study was conducted in a closed-loop system using water (infused with NaCl as salinity manipulator) and oil flowing in a 0.8-inch ID pipe with a length of 27-feet. The study found that salinity effects pressure drop and flow pattern when compared to findings with tap water and oil. Other than that, Besagni and Inzoli [23] conducted a research using a large vertical pipe with a diameter of 94-inch where the effects of NaCl toward flow patterns in counter-current gas liquid flow was investigated. Their findings reported that salinity effects the water and bubble properties which in the end, effects the flow pattern. Therefore, this experimental study of air-brine two-phase flow in horizontal pipe with different air and water flow rates as well as at various salinities is proposed to investigate its effect on flow pattern, pressure drop and liquid holdup in two-phase flow system. Experimental results will also be compared with previously developed correlation models.

1.1 Correlation model

There are several correlation models that have been developed to help researchers and production engineers with crucial information to predict the behavior of multiphase flow in pipes. They are highly recognized and used widely especially in designing pipelines in the petroleum industry.

There are three parameters that are crucial to pressure loss of multiphase flow inside pipes: frictional, hydrostatic, and kinetic energy losses. Among the three parameters, kinetic energy loss is often neglected because of its small value compared to frictional and hydrostatic loss. Hydrostatic pressure loss is however a function of density of the fluids inside the pipe while frictional loss depends on the properties of the fluids and the condition in the pipeline. These parameters are imperative in any design practice [24]. These calculations or correlations can be divided into two main categories which are "Single-phase" and "Multiphase", and in this study, several correlations of multiphase flow will be used and compared with experimental data.

The presence of multiphase flow inside pipes have increased the complexity of the correlations because the parameters and properties are doubled or tripled [25]. Furthermore, the interaction between different phases inside the pipe affects the pressure drop. Thus, to reduce the complexity of multiphase flow correlations, researchers often combine both liquid phase; oil and water to be a single phase while gas is a separate phase. The correlations used are as follows:

1.1.1 Beggs and Brill correlation

There are not many correlations that include inclination of pipes in multiphase flow study. Beggs and Brill correlation however take into account different inclinations from vertical to horizontal pipeline designs. They also developed the correlation by utilizing 1-inch and 1.5-inch pipe sizes which is suitable for comparison in this study. Firstly, to obtain the hydrostatic pressure differences, the flow regime is determined, and from there liquid holdup is calculated based on the flow regime. The density of the mixture can then be determined and used to calculate the pressure difference due to hydrostatic loss. The function of the pressure difference is shown in Eq. 1:

$$\Delta P_{HH} = \frac{\rho_m g}{144 g_c} L \tag{1}$$

where ρ_m is density of mixture, g is gravitational forces, g_c is gravitational conversion factor of 32.174 lbm/lbf.ft/s^2, and L is the length of the pipe.

As for the frictional pressure loss, the calculation depends on the initial gas–liquid ratio and the Fanning friction factor. From this, the properties of the 'Input' gas–liquid mixture is determined and is used to calculate the losses. For this calculation, the non-slip Reynolds number is used. The frictional pressure loss can be calculated using Eq. 2:

$$\Delta P_f = \frac{2 f_{tp} v_m^2 \rho_{NS} L}{144 g_c D} \tag{2}$$

where f_{tp} is gas–liquid friction factor, v_m is mixture velocity,ρ_{NS} is non-slip density which is shown in Eq. 3, D is pipe diameter and L is length of pipe. The sum of both hydrostatic losses and frictional losses is the pressure drop prediction value. The non-slip density is defined in term of input volume fraction (λl) shown in Eq. 4.

$$\rho_{NS} = \rho l \lambda l + \rho g (1 - \lambda l) \tag{3}$$

$$\Delta \lambda_l = \frac{U_{sl}}{U_{sg} + U_{sl}} \tag{4}$$

where U_{sl} is superficial liquid velocity, and U_{sl} is superficial gas velocity.

1.1.2 Lockhart and Martinelli correlation

This model considers two phases flowing independently of one another in the pipe where each phase occupies a certain fraction of the pipe at a given velocity. This made the void fraction to be indispensable. This correlation predicts the pressure drop based on the friction multiplicator for both liquid and gas phases. Martinelli's correlation is defined in Eq. 5 and presented in the form of X.

$$X = \frac{m_l}{m_g}\sqrt{\frac{\rho_g}{\rho_l}} \tag{5}$$

where m_l is liquid mass flowrate,m_g is gas mass flowrate, ρ_l is liquid density, and ρ_g is gas density. From here, the total pressure drop is calculated using Chisholm correlation as shown in Eq. 6 for liquid phase and Eq. 7 for gas phase. With the addition of Chisholm correlation, this correlation has proven to be accurate enough to compare with experimental data according to a similar study done by Kawahara et al. [26].

$$\phi_l = \sqrt{1 + 18X^{-1} + X^{-2}} \tag{6}$$

$$\phi_l = \sqrt{1 + 18X + X^2} \tag{7}$$

1.1.3 Maher et al. correlation

This correlation is based on a homogenous model where the liquid and gas are assumed to be mixed [27]. The main element in this correlation are the relation between two-phase flow viscosity and the conductivity in porous media which in turn produces a new definition for two-phase viscosity mixture (μ_{tp}) which is shown in Eq. 8.

$$\mu_{tp} = \left[(1-x)\mu_l + x\mu_g\right]^{0.94}\left(\frac{1-x}{\mu_l} + \frac{x}{\mu_g}\right)^{1-0.94} \tag{8}$$

where μ_l is liquid viscosity, μ_g is gas viscosity, and x is mass quality. This will then be used to calculate the homogeneous Reynolds number (Re_{tp}) as shown in Eq. 9.

$$Re_{tp} = \frac{G_{tp}D}{\mu_{tp}} \tag{9}$$

where G_{tp} is two-phase mass flux. The Re_{tp} can be used to find gas–liquid friction factor (f_{tp}) using Eq. 10 and the frictional pressure gradient $\left(\Delta P_f\right)$ can be calculated using Eq. 11.

$$f_{tp} = \left(0.79Re_{tp}^{-0.25}\right)^{1.4} + \left[0.17\left(0.69\ln Re_{tp} - 2.2\right)^{-1.5}\right]^{1/0.7} \tag{10}$$

$$\Delta P_f = \frac{G_{tp}^2}{2D\rho_m}f_{tp} \tag{11}$$

In all correlations, frictional losses play an important role in determining the total pressure loss. There are different parameters considered such as acceleration and gravitational losses when comparing Beggs and Brill as well as Lockhart and Martinelli correlation [28]. The acceleration and gravitational losses are neglected in Lockhart and Martinelli correlation as the flow condition is adiabatic and flowing in horizontal condition. Thus, only frictional loss is considered as the total loss. The frictional losses come from the sheer stress acting between the fluid and pipe wall and the shear stress between the two phases [28]. Due to the nature of the flow of liquid and gas, the separated model is used. This method is recognized and used in many industries especially in small pipe size designs [29]. The correlation developed by Maher et al. [27] on the hand, considers the two-phase flow viscosity and mass flux. Apart from that, they also developed a new gas–liquid friction factor function to generate the frictional pressure gradient.

2 Methodology

The experiment was conducted at N10 Heavy Duty Laboratory in the School of Chemical and Energy Engineering, Faculty of Engineering, Universiti Teknologi Malaysia. The overall experimental layout is shown in Fig. 1. The experimental setup is designed as a closed system with open loop facility which comprises of a 1.5-inch inner diameter Schedule 40 carbon steel pipe with a length of 80-feet. This measurement is a scaled down version of pipelines in the industry. The length from the mixing section to the test section is 43-feet, while the length from test section to the separator is 30-feet. The pipe length and diameter are designed accordingly to accommodate flow development at the entrance and exit section of the system. Other equipment incorporated into the flow loop are pumps, metering sections, filters, separator tank, storage tank and instrumentation equipment. The facility is equipped with four transducers placed along the test section. The first pressure transducer is located 34-feet from the mixing point, the second is located just before the test section which is 42-feet from the mixing point, the third is located right after the test section which is 50-feet from the mixing point, and the last is located 58-feet from the mixing point. The data collected by the transducers are then recorded

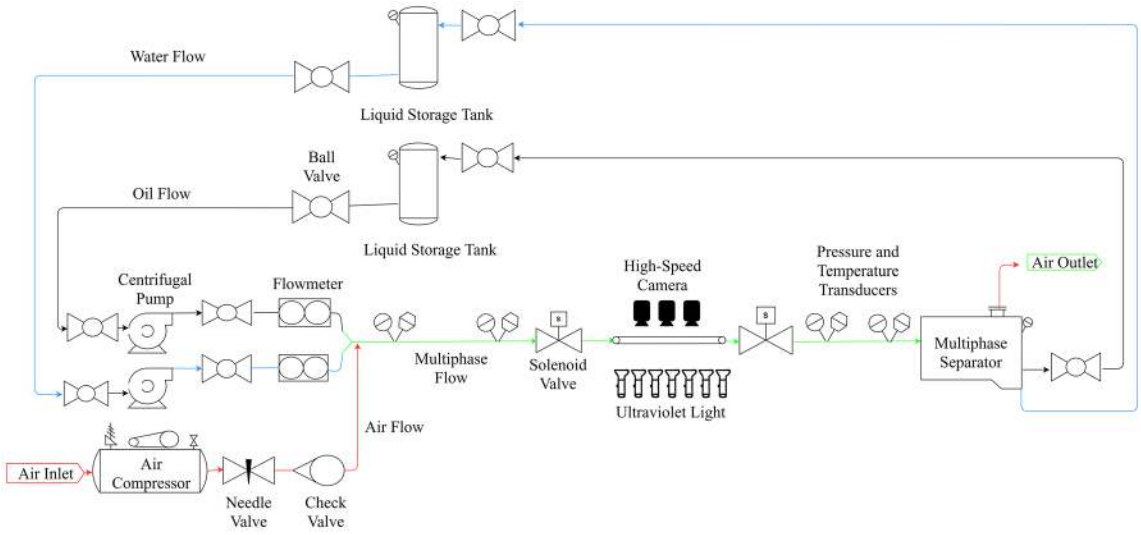

Fig. 1 Schematic diagram of experimental rig setup

by a pressure recorder (Supmea Paperless Recorder, SUP-R9600) in a real-time manner. The experimental setup is designed to run not only single or two-phase flow, but also three-phase flow where a Y-joint is installed as the mixing section. In this study, the setup is used to study horizontal phenomena of two-phase air–water flow behaviors in various fluid flow rates.

The tap water is filtered using 3-stage sand filter which contains zeolite, anthracite, and various sizes silica sand packed in a glass reinforced epoxy vessel with polyethylene inner shell. The filtered water is stored in a water holding tank with volume capacity of 200 L. In the tank, the water is mixed with NaCl to produce brine solution of various concentrations according to NaCl equivalent brine salinity of Malay Basins [30]. A 2-HP centrifugal pump (ProMatic Pump, model PSKT200) controlled by an inverter (Schneider Electric, model ATV312HU15N4) is used to transfer the brine at respective flow rates from the water holding tank to the experimental system. Compressed air is supplied by a standalone air compressor (Swan Air Compressor, model SVP-202). The air system is connected through a high-pressure flexible hose and controlled by a rotameter (maximum air flow = 2.5 m^3/h; minimum air flow = 0.25 m^3/h) and tapped into the experimental system using high-pressure tool fittings. Along the test line is a 7.5-feet long transparent acrylic pipe (ID: 1.5-inch) acting as the test section (observation window) wherein, the flow patterns are observed and recorded. In addition, this line leads to the separator where air is released, and brine is pumped back to the holding water tank via a centrifugal pump.

In this study, the experimental works were conducted at horizontal condition (0°). The temperature was kept constant at ambient temperature, 30 °C with the help of insulated pipeline throughout the flow loop. The superficial velocities of air ranges from 0.01 to 0.609 m/s and the superficial velocities for brine ranges from 0.5 to 3.0 m/s. The range of superficial velocities were chosen to simulate turbulent flow throughout the pipe.

2.1 Test section

The test section is comprised of a transparent acrylic pipe that is 7.5-feet long with an internal diameter (ID) of 1.5-in. The test section is used for flow pattern visualization and liquid holdup. A high-speed Sony digital camera model FDR-X3000R with the capability to capture high frame per second (FPS) is placed perpendicularly to the test section to detect and capture the flow patterns of the fluid when flowing in the pipe. It is located at the midway of the last part of the test section. To assist in the observation and determination of flow pattern, fluorescent powder (Laboratory Reagent, $C_{20}H_{12}O_5$) is mixed in the brine to give it a fluorescent colour. UV lights intensify the fluorescent colour and improve the appearance of the flow pattern when captured by the camera. Other than that, two solenoid valves or quick closing valves (Watts Regulator) with maximum pressure of 125 psi are installed at both ends of the transparent acrylic pipe. The solenoid valves are used to trap the fluids for measuring liquid holdup which are collected using the drain valves fixed at both ends of the test section. Both valves must be closed simultaneously when the two-phases are flowing in the pipe during the experiment. The most crucial step in this method is the synchronized closing of valves at both ends of the test section because with every 20 ms missed; the resulting

error will be less than 1% [31]. If the two solenoid valves are not synced to close at the same time, this may lead to an error where the test section may be filled completely with stagnant fluid. There are also a number of previous researchers who reported using the same method [31–38].

Moreover, the test section of the rig is facilitated with four thermocouple probes (Heattemps, type HT-1; accuracy: ± 2.4 °C from -200 °C to 1200 °C) which are connected to temperature indicators (CAHO, model SR-T602) to display the detected temperatures (0 °C to 1000 °C) with accuracy of ± 0.5 °C and resolution of 0.1 °C. Pressure is measured using four pressure gauges (WIKA Instrumentation) with accuracy of 1.4% and was recorded using pressure recorder (Supmea Paperless Recorder, SUP-R9600).

Liquid holdup is defined as the ratio of trapped water to the total volume of removable spool piece. Liquid holdups are measured using a 2000 ml graduated measuring cylinder. As the test fluid flows through the test section (transparent acrylic pipe), the two solenoid valves are closed to trap the fluid in the removable spool piece. Solenoid valve is chosen because it is designed to automatically close both ends of the test section at a fast rate. According to Oddie et al. [31], synchronized closing of valves at both ends must be done simultaneously because with every 20 ms missed, a resulting error of less than 1% will occur in the measurements. The test focuses on air and three different brine salinities (1000 ppm. 15,000 ppm and 30,000 ppm) which represents the reservoir brine salinity within the Malay Basin [30].

3 Results and discussion

Three different sodium chloride concentrations were added to the liquid phase. The properties of brine and Reynolds number are tabulated in Table 1. All the tests conducted were in turbulent regime.

3.1 Flow pattern

A videography study was carried out during the experiment for each varying condition. Based on the flow classifications proposed by previous researcher [39–45], the flow patterns observed could be grouped into four main types and subdivided into more detailed classifications as shown in Table 2.

Table 2 Type of flow patterns observed

Type	Sub-type
Stratified	(a) Smooth
	(b) Wavy
Intermittent	(a) Plug
	(b) Slug
	(c) Pseudo-slug
Dispersed bubble	–
Mixed flow	(a) Slug + Annular
	(b) Plug + Slug
	(c) Slug + Thin annular

3.1.1 Stratified flow

Stratified flow or also known as segregated flow is a type of flow where a clear segregation between phases can be seen and that of which produces a definitive interface between them [45]. There are two types of stratified flow, namely stratified smooth and stratified wavy. This type of flow is highly dependent on the gravitational forces acting on them where the phases inside the pipe are segregated based on their density, lighter phase flow above the heavier phase [46]. This type of flow usually occurs in low liquid and gas superficial velocity which leads to a clear distinct interface formed throughout the test section. Figure 2 shows a stratified smooth flow where the air and brine are clearly separated by an undisturbed horizontal interface. The liquid and gas are fully stratified in this regime [47].

As superficial gas velocities increase, the smooth horizontal interface become agitated and destabilized resulting a wavy surface flowing in the direction of the flow between the gas–liquid interface [46]. However, the amplitude of the wave are not large enough to touch the ceiling of the pipe or break the air flow [41]. This type of flow is known as stratified wavy as shown in Fig. 3. The waviness on the surface between the brine and air are caused by drag of the gas passing on top of the brine [48].

Table 1 Test liquid properties

NaCl con. (ppm)	Density (kg/m^3)	pH	Dial reading at Shear rate (1022 s^{-1})	Newtonian viscosity (cp)	Reynolds number at different U_{sw} (ms^{-1})					
					0.5	1.0	1.5	2.0	2.5	3.0
1000	1001.75	6.52	3.0	1.005	8481.5	16,963	25,444.5	33925.9	42407.4	50888.9
15000	1006.54	6.39	3.5	1.276	7304.6	14609.2	21913.8	29218.4	36523	43827.6
30000	1012.53	6.24	4.0	1.756	6429.6	12859.1	19288.7	25718.3	32147.8	38577.4

Fig. 3 Stratified wavy flow

Fig. 2 Stratified smooth flow

3.1.2 Intermittent

Intermittent flow is a type of flow that is usually formed after stratified flow when the superficial velocity of gas is increased. The increase in gas flow rate causes an increase in drag on the surface between air and brine which then produces waves large enough to wet the top of the pipe hence separating the gas flow. This causes bubble to form on top of the brine and flows intermittently as air flow is constantly engulfed by the brine. This study found that intermittent flow can be broken down into three types of flows which are plug, slug and pseudo-slug. The differences between them relies on the void fraction or slug size and the degree of turbulence formed [49]. Plug flow or also known as elongated bubble are formed at lower gas and liquid superficial velocity compared to slug and pseudo-slug flow. In this flow regime, elongated bubble can be seen flowing on top of continuous brine flow. The diameter of the elongated bubbles is significantly smaller than the pipe diameter. These bubbles are separated by brine that engulfs the whole inner wall of the pipe and in between the bubbles causing them to move intermittently between the brine. This flow can be seen in Fig. 4a and b.

On the other hand, slug flow is formed at higher superficial gas velocities than plug. The tail of the elongated bubble in slug flow can be seen flowing on top of brine flow continuously. The diameter of the elongated bubble for slug flow is significantly smaller than the pipe inner diameter but slightly larger than the bubble diameter for plug flow. In contrast to plug flow, these bubbles are not separated by brine as a slim bubble connects two larger bubbles. The same flow is described by Yang et al., [50] in their studies. This flow is captured in Fig. 5.

Fig. 5 Slug flow

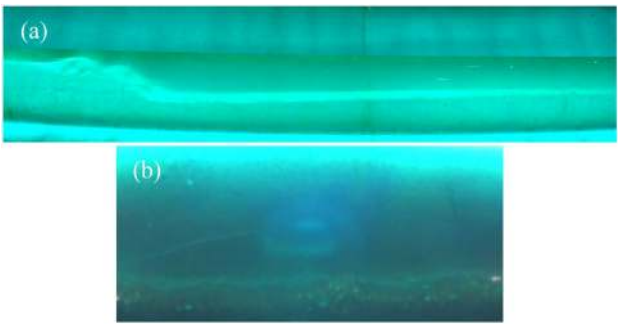

Fig. 6 **a** Pseudo-slug flow **b** Absence of annular film from top view

Meanwhile, this study found that pseudo-slug forms at higher superficial gas velocity than slug. The elongated bubbles and structures are similar to slug flow, but the waves amplitude is larger [49]. Other than that, the starting and ending waves are not similar in terms of shapes. This can be caused by the extremely aerated structure formed at the amplitude due to high gas penetration into the liquid slug body [51]. This flow is captured in Fig. 6a. For stratified and intermittent flow, water film is absent on top of the pipe as shown in Fig. 6b.

3.1.3 Dispersed bubble

Dispersed bubble or also known as bubbly flow is usually formed at higher liquid velocities. In lower velocity, the liquid tends to be pulled down by gravitational force hence flowing in stratified flow instead of dispersed bubble. On the contrary, dispersed bubble refers to small spherical bubbles flowing throughout the body of the fluid inside the pipe. As mentioned, horizontal flow is influenced mainly by buoyancy and gravitational forces. It is observed

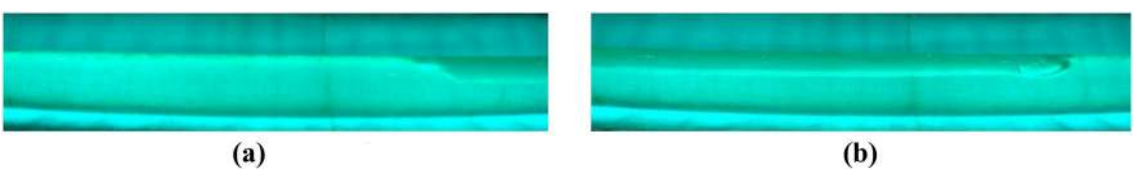

Fig. 4 **a** Plug flow end and **b** Plug flow Start

Fig. 7 Dispersed buble flow

that the bubbles start dispersing at the upper half of the pipe, however, this distribution only happens in lower Reynolds number. In higher Reynolds number, the bubbles are observed to be distributed throughout the pipe's cross-section and this is supported by Kong and Kim [2]. This flow is captured in Fig. 7.

3.1.4 Mixed flow

Mixed flow is identified as transitional flow between flow regime. In this study, three types of mixed flows are captured, namely; Plug + Slug, Slug + Thin Annular, and Slug + Annular. Plug + Slug flow is usually observed between plug and slug flow. This type of flow regime is different from plug and slug flow respectively because both of the flow co-exist in the same flow line alternating with each other. First a plug flow is observed, followed by a slug flow then ends with another plug flow. This is different from a normal plug or slug flow as only one type of flow alternating with a bodily fluid is observed. This type of flow is shown in Fig. 8, where the start of plug flow is shown in Fig. 8c, the slug body in Fig. 8b, and the plug ends in Fig. 8a.

Slug + Thin Annular flow is observed between the formation of slug and annular flow. This type of flow happens when the superficial velocity is high. Like slug flow, the elongated bubbles in this flow are seen flowing on top of the brine continuously but the bubbles are covered by a thin layer of liquid on the top wall of the pipe. This thin layer of liquid is observed to be flowing together with the bubbles and brine. This flow is captured in Fig. 9a. Figure 9b shows a thin layer of water flowing on top of the pipe.

When gas velocity is increased, the thin brine layer thickened forming the Slug + Annular flow. Other than that, the elongated bubble or void seemed to be bigger and its presence became more frequent compared to

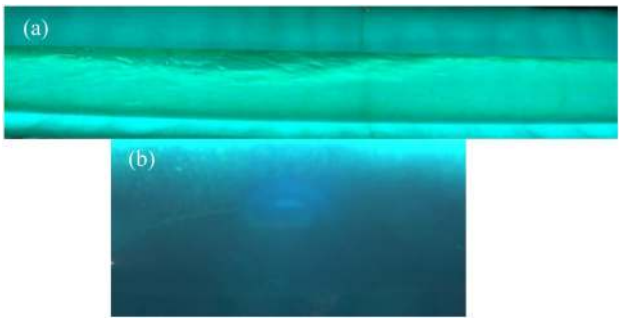

Fig. 9 **a** Slug + Thin Annular, **b** Thin Annular from top view

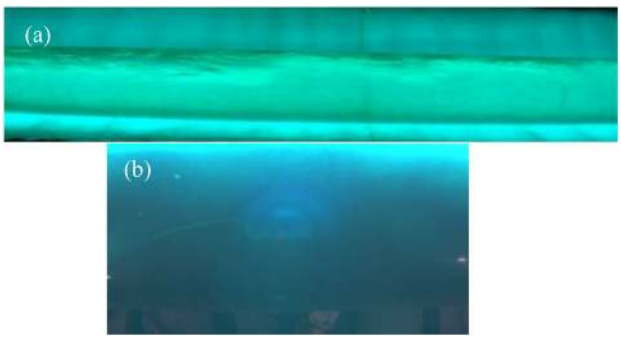

Fig. 10 **a** Slug + Annular, **b** Annular from top view

Slug + Thin Annular flow. However, the elongated bubble is seen to be on the top half of the pipe cross-section due to gravitational forces and buoyancy [2, 47, 52]. This flow is captured in Fig. 10a. In this case, the presence of water film is thicker on top of the pipe which is shown in Fig. 10b where the image is more opaque.

3.2 Flow pattern map

Flow pattern map is a two-dimensional chart that maps the most likely flow to be found at certain liquid and gas superficial velocity in a fixed pipe size. This map is simple but very useful in predicting the flow condition and regimes at different flow conditions [53]. This is very significant in designing and operating any multiphase flow system. In this study, the flow map is plotted based on

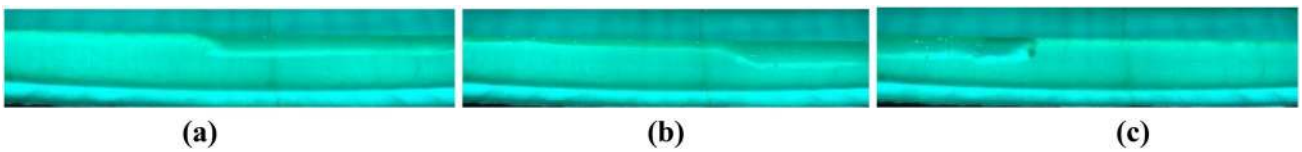

Fig. 8 Plug + Slug flow: **a** End, **b** Middle, and **c** Start

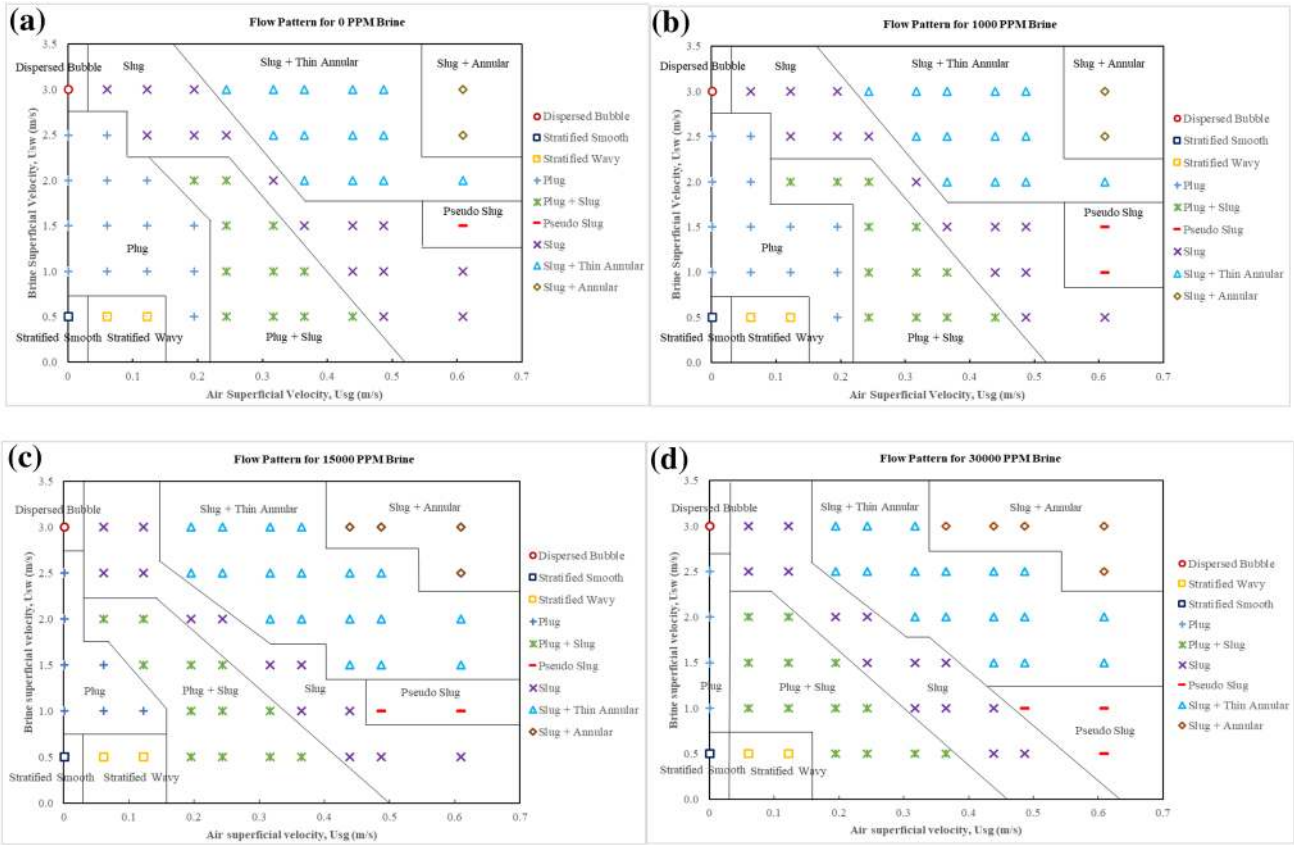

Fig. 11 Transitional boundaries for **a** 0 PPM **b** 1000 PPM brine **c** 15,000 PPM brine **d** 30,000 PPM brine

the experimental visual data from a High-Speed Camera. The videos and pictures are captured from the gas-brine (Two-Phase flow) flowing in 1.5-inch carbon steel pipe in horizontal conditions. Based on the flow pattern mapped out in Fig. 11a–d, with brine salinity of 0 ppm, 1000 ppm, 15,000 ppm and 30,000 ppm, it is proven that the flow pattern changes as the brine salinity changes. It is observed that for all brine salinities, as the superficial flow velocity of gas, U_{sg} and superficial flow velocity of water, U_{sw} increases from 0.01 m/s to 0.609 m/s and from 0.5 m/s to 3.0 m/s respectively, the flow pattern transitions from stratified to intermittent to mixed flow. Stratified flow is observed at $U_{sg} \leq 0.122$ m/s and $U_{sw} \leq 0.5$ m/s in all the brine salinity tested. Within that range, it is also observed that a transition from stratified smooth to stratified wavy happened between U_{sg} of 0.061 m/s and 0.122 m/s. As salinity increases, there are no significant changes to the transition line. As the U_{sw} and U_{sg} increases, the stratified flow changes to intermittent flow followed by dispersed bubble flow which correlates to the flow pattern map proposed by previous researchers [16, 40, 41, 44]. There are three types of flow observed in intermittent flow, namely plug, slug and pseudo-slug. For plug flow, it is observed at region of $U_{sg} \leq 0.195$ m/s and $U_{sw} \leq 2.5$ m/s for 1000 ppm salinity. However, it is observed that as the salinity increased, the plug flow transition line shift towards lower U_{sg} but there are no significant shift in U_{sw}. For slug flow, the transition line is observed to be at medium to high U_{sg} and U_{sw} region. For 1000 ppm salinity, slug flow can be observed at $U_{sg} \geq 0.487$ m/s at U_{sw} of 0.5 m/s. However, as U_{sw} increases, the transition line moves diagonally toward the left of lower U_{sg}. The same flow can be observed at U_{sw} of 2.5 m/s and U_{sg} of 0.122 m/s in the same salinity. Furthermore, as the salinity increases, the transition line for slug flow shifts towards lower U_{sg} but did not show any significant shift in U_{sw}. For pseudo-slug, the flow can be seen right after slug flow at $U_{sg} \geq 0.487$ m/s and $U_{sw} \leq 2$ m/s. This flow is observed at U_{sg} 0.609 m/s with U_{sw} between 1.0 m/s and 1.5 m/s for 1000 ppm and at U_{sg} 0.609 m/s with U_{sw} between 1.5 m/s and 2.0 m/s for 0 ppm. However, this flow can be observed at lower U_{sg} of 0.487 m/s in 15,000 ppm salinity. As salinity increases, the transition line shifted slightly towards lower U_{sg} and U_{sw}.

Dispersed bubble flow can be observed at higher U_{sw} but low U_{sg} region. In every salinity tested, dispersed bubble flow is observed at $U_{sg} \leq 0.061$ m/s and $U_{sw} \geq 3.0$ m/s. Plug + Slug flow is observed between the plug and slug flow. It is identified that this type of flow is a transitional

flow. In 1000 ppm salinity, the transition line for this flow is observed to be between U_{sg} of 0.294 m/s and 0.439 m/s at U_{sw} of 0.5 m/s. However, at U_{sw} 2.0 m/s, the transition line appears at a lower U_{sg} of 0.061 m/s and 0.122 m/s. The transition line appears at a higher U_{sg} which is between 0.122 m/s and 0.0.195 m/s at U_{sw} 2.0 m/s for 0 ppm. The transition line move toward lower U_{sg} as the U_{sw} increases. In terms of increasing salinity, a significant transition line shift can be seen towards lower U_{sw}, and only a slight shift towards lower U_{sg}. For Slug + Thin Annular, this is a transitional flow between slug and slug-annular flow. This flow occurs at medium to high U_{sg} and U_{sw} region. For low U_{sw} of 1.5 m/s, the flow is observed starting at U_{sg} of 0.439 m/s in salinity brine of 1000 ppm. However, at higher U_{sw} of 2.5 m/s, the flow started to develop at U_{sg} of 0.195 m/s. From observation, the transition line shifts toward lower U_{sg} as U_{sw} increases. For 15,000 and 30,000 ppm, this flow can be observed at a much lower U_{sw} of 1.5 m/s. In terms of salinity, the transition line shifts toward lower U_{sw} and U_{sg} as salinity increases, but there are no significant changes between 15,000 and 30,000 ppm. At the highest U_{sg} of 0.69 m/s and at $U_{sw} \geq 2.5$ m/s, a Slug-Annular flow was observed in all three salinities. As the brine salinity increases, the transition line has shifted towards lower U_{sg} (at U_{sw} of 3.0 m/s) where the flow is developed at $U_{sg} \geq 0.439$ m/s for 15,000 ppm and $U_{sg} \geq 0.365$ m/s for 30,000 ppm. There is no shift in the transition line for U_{sw} of 2.5 m/s.

3.3 Pressure drop

Figure 12a–d presents pressure drop data obtained with brine concentrations of 0 ppm, 1000 ppm, 15,000 ppm and 30,000 ppm respectively. The data are plotted against the air superficial velocity, U_{sg}, for different brine superficial velocities, U_{sw}. Based on the figures, it is shown that the pressure drop increases as U_{sg} and U_{sw} increases for all concentrations. However, as the U_{sw} increases along with U_{sg}, there are significant differences in pressure drops for each brine concentration which leads to a deduction as expected that, brine salinity affects the pressure drop.

According to Fig. 12a to d, pressure drop showed an increasing trend for superficial water velocities, U_{sw} of 0.5 to 3.0 m/s with increasing air superficial velocities, U_{sg} from 0.01 to 0.6 m/s. Based on Fig. 12a–b, at U_{sw} of 1.5, 2.0, 2.5, and 3.0 m/s with respect to U_{sg} 0.6 m/s, increase in pressure drop percentages by 83.3%, 75.0%, 58.8%, and 57.5% respectively for brine salinity of 0 ppm was recorded; for

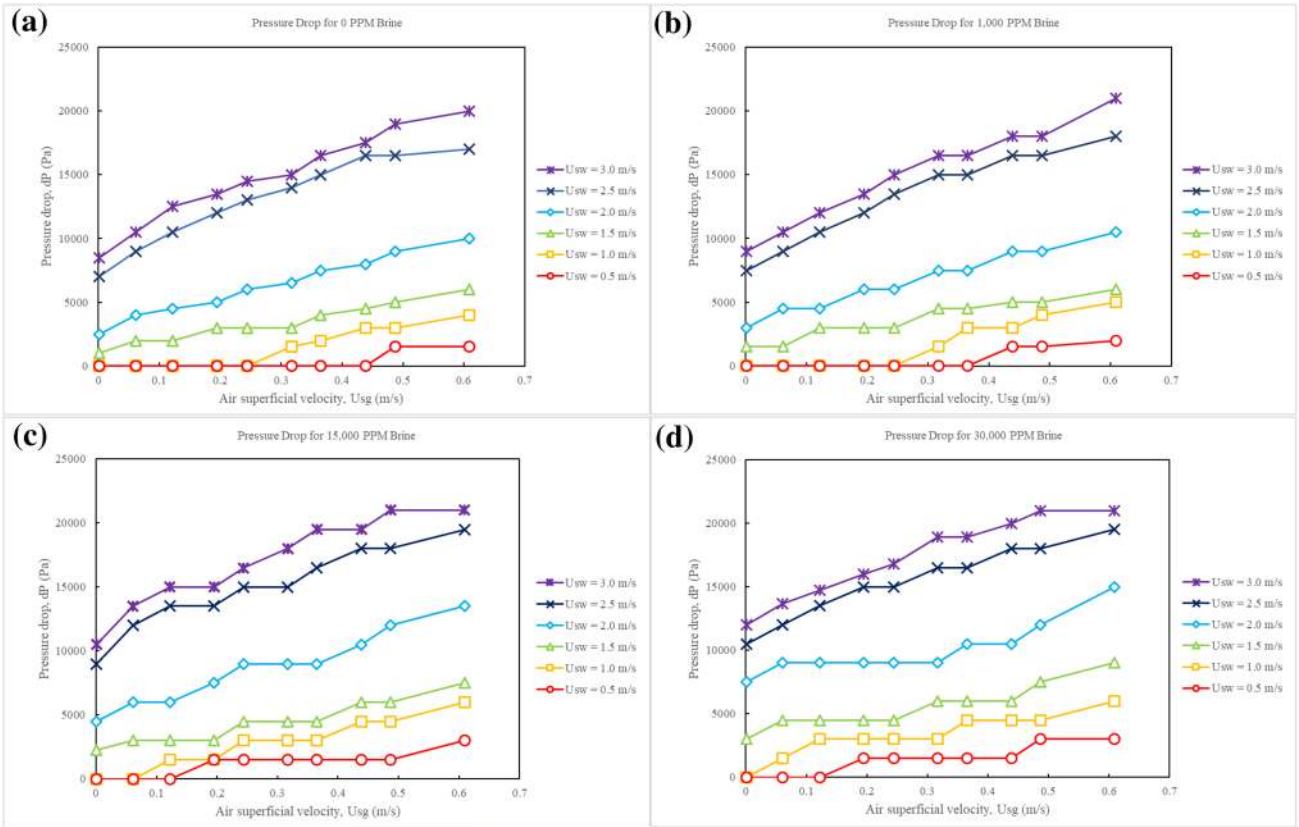

Fig. 12 Pressure drop for **a** 0 PPM **b** 1000 PPM brine **c** 15,000 PPM brine **d** 30,000 PPM brine

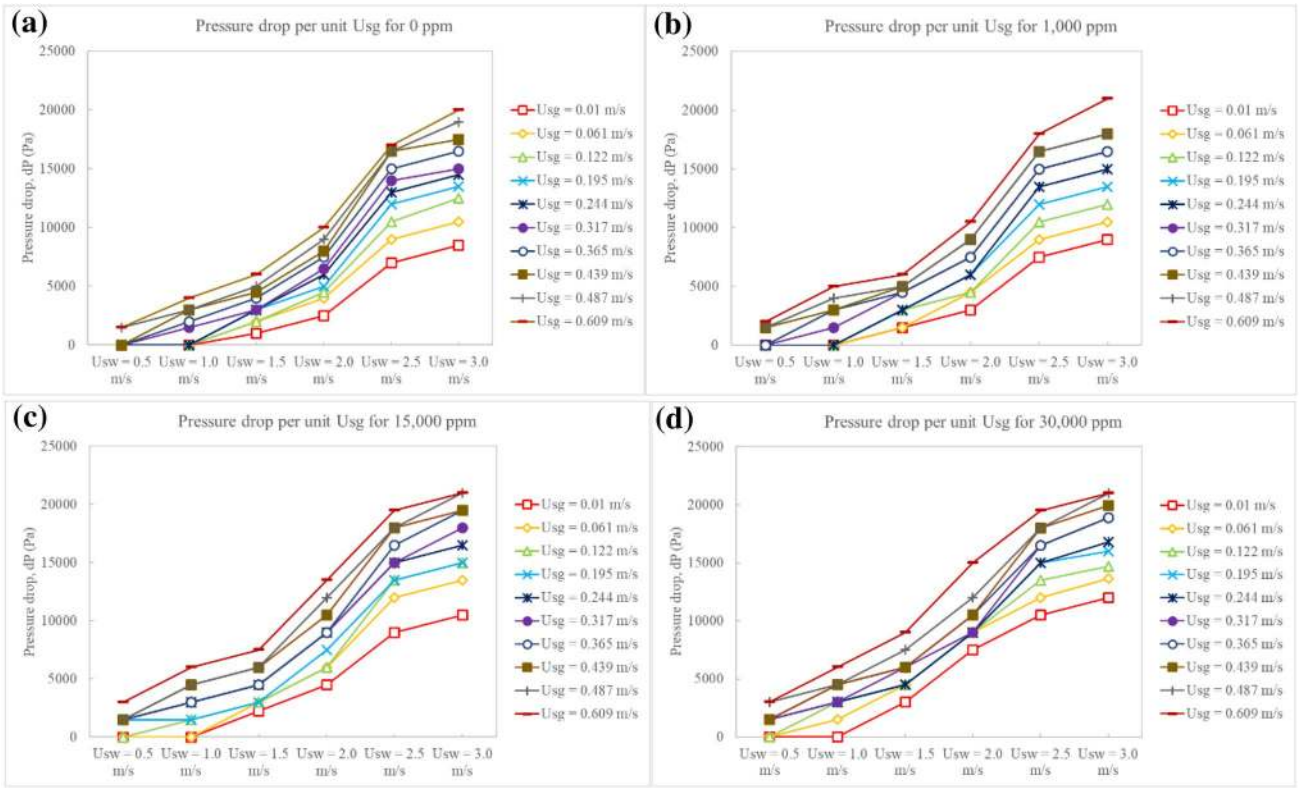

Fig. 13 Pressure drop per unit U_{sg} for **a** 0 PPM **b** 1000 PPM brine **c** 15,000 PPM brine **d** 30,000 PPM brine

brine salinity of 1000 ppm, the pressure drop percentages increase by 75.0, 71.4, 58.3, and 57.1% respectively. Meanwhile based on Fig. 12b, the pressure drop increment percentage for a higher brine salinity of 15,000 ppm were 70, 66.7, 53.9, and 50% for U_{sw} of 1.5, 2.0, 2.5, and 3.0 m/s respectively at air superficial velocities 0.6 m/s. On the other hand, the highest brine salinity of 30,000 ppm as shown in Fig. 12c tested in this study showed the lowest pressure drop increment percentage compared to lower brine salinities. The tests recorded a pressure drop increase of 67.7%, 50%, 46.2%, and 42.9% as the air superficial velocities 0.6 m/s. In the meantime, all brine salinities recorded a gradual increase of pressure drop which starts from 0 Pa at zero U_{sg} to a range of 1000 to 4000 Pa as the U_{sg} increases from 0.01 to 0.6 m/s for U_{sw} of 0.5 and 1.0 m/s as shown in Fig. 13a–d. At U_{sg} 0.01 m/s and U_{sw} 3.0 m/s, the pressure drop ratios recorded for 15,000 ppm, 10,000 ppm and 0 ppm were 0.125, 0.25, and 0.29 times less than what was recorded for 30,000 ppm respectively. However, as the U_{sg} increases, the pressure drop ratio decreases. This is observed at U_{sg} 0.439 m/s and U_{sw} 3.0 m/s where pressure drop ratios recorded for 15,000 ppm, 10,000 ppm and 0 ppm were only 0.02, 0.1, and 0.12 times less than what was recorded for 30,000 ppm respectively. This shows that higher salinity recorded higher average pressure drop compared to lower salinity. The reason behind this is that heavier liquid density will have more resistance and friction when flowing compared to lower density fluids. This is also because the denser the fluid, the higher the viscosity because there are more NaCl particles present in the fluid. Liquid with higher viscosity tend to have higher drag compared to lower viscosity fluids and this in turn rises the pressure drop in the system [54]. According to Wang [55], U_{sw} has more significant impact on pressure drop compared to U_{sg} as it is influenced by gravitational forces. According to Kawahara et al. [56], pressure drop is highly affected by flow patterns of the flow, density, and velocity. The flow pattern when transition from stratified to intermittent to dispersed bubbles to mixed flow shows increment in pressure drop. The differences in U_{sw} and U_{sg} are due to different brine concentration and air input fraction which affects the flow pattern. From the result shown in Fig. 12a to d, it is observed that pressure drop increases as U_{sg} increases. There is some major fluctuation of pressure detected when slug flow was observed. The large elongated bubbles flowing intermittently seemed to cause the fluctuation. This is also supported by Kee et al. [48] and Anumbe [53]. The condition is due to increase in

U_{sg}, which results in increase of air fraction available in the pipeline. According to Al-Wahaibi et al. [57], the concentration of liquid affects pressure drop of the flow. The concentration here is related closely to density; thus, based on the statement, we can conclude that brine concentration or density affects the pressure drop. Although there were no significant changes observed at lower U, the pressure drop increases as U_{sw} increases. This experiment deduced that salinity and flow patterns transition affect pressure drop of the system.

3.3.1 Pressure drop comparison

The 1000 ppm brine salinity was selected for the pressure drop comparison between experimental data and previous correlations. From the trend, there are similarities observed for all three correlations where the pressure drop increases as U_{sw} and U_{sg} increases. According to Fig. 14, there are large disparities when using the Beggs and Brill correlation. For example, the pressure drop at U_{sg} of 0.609 m/s and U_{sw} of 0.5 m/s recorded the smallest percentage difference of 0.16%. The highest percentage difference recorded was 56.07% at U_{sw} of 1.5 m/s. The average difference for all six U_{sw} at U_{sg} of 0.609 m/s is 29.96%.

The Lockhart and Martinelli correlation predicted better accuracy with experimental results in this study, as shown in Fig. 15. The difference between experimental and calculated values of pressure drops are not far off. The lowest recorded percentage difference at U_{sg} 0.609 m/s is 5.03% on U_{sw} 2.5 m/s. The highest percentage difference is 19.04% recorded at U_{sg} 0.609 m/s and U_{sw} 3.0 m/s. The average difference between experimental data and Lockhart and Martinelli correlation is at U_{sg} 0.609 m/s is 16.35% which is a better prediction compared to Beggs and Brill correlation.

Maher et al. correlation gave the best accuracy which is shown in Fig. 16. This correlation prediction is not far off from Lockhart and Martinelli. At U_{sg} 0.609 m/s, the lowest and the highest percentage difference recorded were 1.22% at U_{sw} 2.5 m/s and 36.24% at U_{sw} 1.5 m/s respectively. The average difference for all six U_{sw} at U_{sg} of 0.609 m/s is 13.43% which is the best average percentage difference between the three correlations.

Figure 17 presents the comparisons between the predicted pressure drop from all three correlations to the experimental data. It is observed that Maher et al. correlation gave the best predictions compared to the correlations by Beggs and Brill and Lockhart and Martinelli.

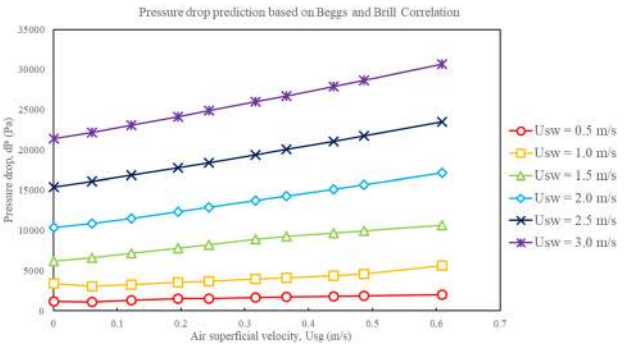

Fig. 14 Pressure drop by Beggs and Brill correlation

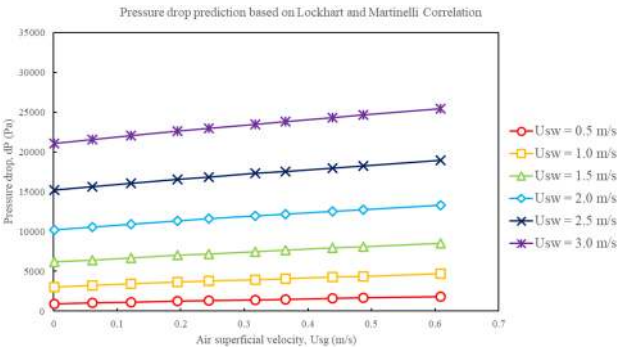

Fig. 15 Pressure drop by Lockhart and Martinelli correlation

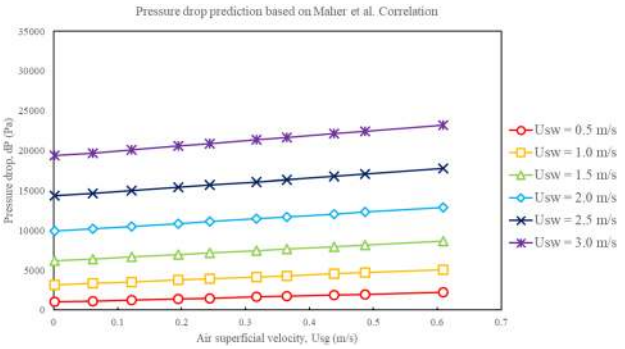

Fig. 16 Pressure drop by Maher et al. correlation

Majority of the data for all three correlations predicted values that were higher than the experimental values. Maher et al. correlation shows the least discrepancies while Beggs and Brill correlation gave the largest errors. Table 3 lists the percentages of data within 15% and 35% of error band. The highest percentage of data points recorded within the 35% error band is from Maher et al. correlation with 36.67%, followed by Lockhart and

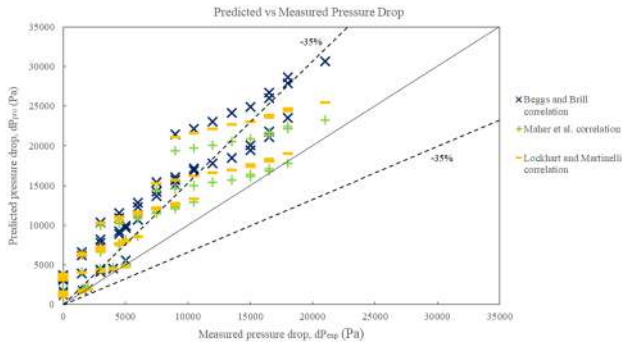

Fig. 17 Predicted versus measured pressure drop

Table 3 Percentage of data within 15% and 35% error bands

Model/Correlation	Percentage within ± 15%	Percentage within ± 35%
Beggs and Brill	5.00	13.33
Lockhart and Martinelli	15.00	25.00
Maher et al.	23.33	36.67

Martinelli's correlation with 25% and the least is from Beggs and Brill's correlation with 13.33%. The table also shows the percentage of data points recorded within the 15% error band.

3.3.2 Mean absolute relative deviation (MARD) and mean relative deviation (MRD)

The behavior of all the correlations when compared to the actual data are tabulated in terms of Mean Absolute Relative Deviation (MARD) and Mean Relative Deviation (MRD) as shown in Table 4. All of the correlations produced MARD and MRD results of over 50% and the lowest recorded MARD and MRD is from the correlation by Maher et al..The high percentage is caused by large discrepancies between experimental and predicted data especially at U_{sw} 1.5 m/s and 2.0 m/s for all three correlations. The equation for MARD and MRD are shown in Eqs. 12 and 13, respectively.

$$MARD = \frac{1}{N}\sum_{i=1}^{N}\left|\frac{\Delta P_{(i)pred} - \Delta P_{(i)exp}}{\Delta P_{(i)exp}}\right| \quad (12)$$

$$MRD = \frac{1}{N}\sum_{i=1}^{N}\frac{\Delta P_{(i)pred} - \Delta P_{(i)exp}}{\Delta P_{(i)exp}} \quad (13)$$

where N is the number of calculation points, $\Delta P_{(i)pred}$ is predicted pressure drop, $\Delta P_{(i)exp}$ is experimental pressure drop.

Table 4 MARD and MRD values for experimental data

Model/correlation	MARD	MRD
Beggs and Brill	71.89	71.16
Lockhart and Martinelli	58.86	53.76
Maher et al.	51.95	58.35

3.4 Liquid holdup

Based on the plots in Fig. 18a–d, it can be observed that as U_{sw} increase, H_w increase. According to Kuntoro et al., [48], the liquid holdup is highly dependent on the flow pattern and water input fraction. For brine salinity of 1000 ppm, 15,000 ppm and 30,000 ppm, at low U_{sw} and low U_{sg}, the flow pattern observed is stratified flow. As the U_{sw} increases as well as the U_{sg}, intermittent and mixed flow is observed. The overall trend for each brine salinity is that the H_w decreases as the U_{sg} increases at a constant U_{sw}. This correlates to a study done by Dabirian et al. [5] where they stated that H_w decreases as the U_{sg} increases at constant U_{sw} and H_w increases as U_{sw} increases at constant U_{sg}. However, in this study, the H_w showed almost the same values and pattern which were in the range of 70–86% for U_{sg} below 0.122 m/s for all brine salinities. For U_{sg} above 0.122 m/s, the H_w for all brine salinities show a decreasing trend but in slightly different patterns. Based on Fig. 18a, as the U_{sw} increases from 0.5 to 3.0 m/s, the H_w decreases from 64.40 to 34.4% for liquid with brine salinity of 0 ppm. Other than that, Fig. 18b, brine salinity of 1000 ppm shows that as the U_{sw} increases from 0.5 to 3.0 m/s, the H_w decreases from 64.6 to 32%. Meanwhile, brine salinity of 15,000 ppm (Fig. 18c) shows a decrease in H_w from 65.1% to 26.6% as the U_{sw} increase from 0.5 to 3.0 m/s. Lastly, brine salninity of 30,000 ppm (Fig. 18d) shows a decrease from 69.5 to 25.2% as the U_{sw} increase from 0.5 to 3.0 m/s. A more detailed percentage difference in H_w is shown in Fig. 19. Results show that higher salinity fluid (30,000 ppm) produced a higher percentage difference of H_w compared to lower salinity fluids (1000 and 15,000 ppm) when $U_{sw} < 1.5$ m/s. On the contrary, lower salinity fluid (1000 ppm) produced a higher percentage difference of H_w compared to higher salinity fluids (15,000 and 30,000 ppm) when $U_{sw} > 2.0$ m/s. This difference may be caused by the different flow patterns flowing as if the flow is more gas dominant. Furthermore, results also show that the percentage difference of H_w did not decrease any further or significantly between U_{sw} 2.5 and 3.0 m/s. This is because as the U_{sw} increase, large amounts of fluid cover most of the pipe volume thus no significant changes in percentage difference of H_w is recorded.

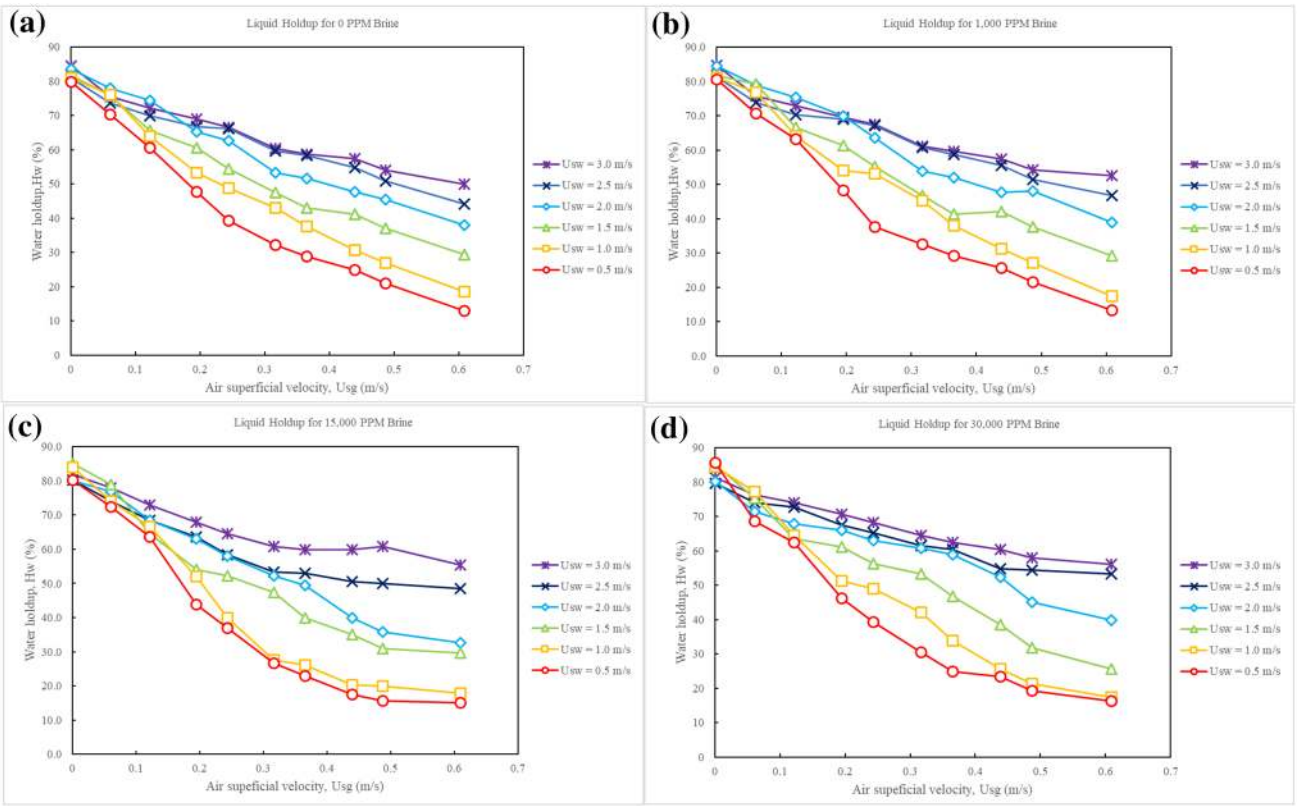

Fig. 18 Liquid holdup for **a** 0 ppm **b** 1000 PPM brine **c** 15,000 PPM brine **d** 30,000 PPM brine

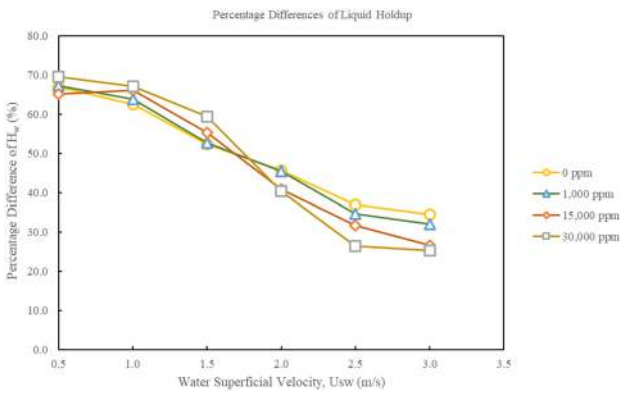

Fig. 19 Percentage difference of liquid holdup

4 Conclusions

The findings of this experimental study of two-phase gas-brine flow in a horizontal system is compared with previous correlation models and the conclusions are summarised below:

1. Different flow patterns under various U_{sg} and U_{sw} were observed during the experiment, namely stratified smooth, stratified wavy, plug, slug, plug + slug, pseudo-slug, dispersed bubbles, slug + thin annular, and slug + annular. A combination of flow was identified where a combination of plug, slug and thin annular flow was present. Different concentration of brine exhibits different flow patterns at different superficial fluid velocities. The flow pattern map generated obey the flow transitions of previous studies. This study reports significant effect of salinity towards the transition lines of flow. However, the findings also show that the flow pattern map is not entirely dependent on salinity, but also by other factors.
2. Pressure drops at lower U_{sg} and U_{sw} is the lowest and as the velocity increases, the pressure drop increases as well. However, when brine salinity increases the pressure drop decreases. This concludes that salinity affects the pressure drop of the system.
3. The correlation developed by Maher et al. produced the best prediction among the three correlations when compared to experimental data. The prediction is however not far from the correlation by Lockhart and Martinelli. Lockhart and Martinelli correlation performed better in predicting the pressure drops in regard to this experimental study compared to Beggs and Brill correlation. This is because Lockhart and Martinelli correlation included the mass flowrate of liquid and gas

separately in their equation and with the addition of the Chrisholm correlation, a more accurate prediction of pressure drop to the experimental value is obtained. However, Maher et al. correlation was more detailed as they included factors such as two-phase viscosity mixture and gas–liquid friction factor.

4. H_w analysis were done by plotting H_w versus U_{sg}. H_w decreases as the U_{sg} increases at constant U_{sw}. This is due to increase in U_{sg} which leads to an increase in air-brine ratio in the pipeline which also leads to the reduce in the amount of H_w in the test section. At increasing brine salinity, as U_{sw} increases along with U_{sg}, the liquid holdup increases. Liquid holdup percentage decreases from 64.4 to 34.4%, 64.6 to 32%, 65.1 to 26.6%, and 69.5 to 25.2% for brine salinity of 0 ppm, 1000 ppm, 15,000 ppm, and 30,000 ppm respectively as the U_{sw} increase from 0.5 to 3.0 m/s.

Acknowledgements The authors would like to express their gratitude to the Ministry of Higher Education, Malaysia and Universiti Teknologi Malaysia for funding this project under the Research University Grants Vote Number 14H83, and the Contract Research DTD with reference numbers PY2016/06,266, PY/2017/01823 and PY/2018/03001.

Compliance with ethical standards

Conflicts of interest On behalf of all authors, the corresponding author states that there is no conflict of interest.

References

1. Zubir MA, Zainon M (2011) Two-phase flow behaviour and pattern in vertical pipes. J Appl Sci 11(9):1491–1500. https://doi.org/10.3923/jas.2011.1491.1500
2. Kong R, Kim S (2017) Characterization of horizontal air–water two-phase flow. Nucl Eng Des 312:266–276. https://doi.org/10.1016/j.nucengdes.2016.06.016
3. Abdul-Majeed Ghassan, Al-Mashat Ali (2019) A unified correlation for predicting slug liquid holdup in viscous two-phase flow for pipe inclination from horizontal to vertical. SN Appl Sci. https://doi.org/10.1007/s42452-018-0081-0
4. Ihara M, Yanai K, Takao S (1995) Two-phase flow in horizontal wells. Soc Pet Eng. https://doi.org/10.2118/24493-PA
5. Dabirian R, Padsalgikar A, Mohammadikharkeshi M, Mohan RS, Shoham O (2018) The effects of phase velocities and fluid properties on liquid holdup under gas-liquid stratified Flow. In: SPE Western regional meeting proceedings.https://doi.org/10.2118/190097-ms
6. Fanchi JR (2018) Wells. In: Fanchi JR (ed) Principles of applied reservoir simulation, 4th edn. Gulf Professional Publishing, Houston, pp 139–162
7. Lim ZW, Goh KL (2019) Natural Gas industry transformation in peninsular Malaysia: the journey towards a liberalised market. Energy Policy 128:197–211. https://doi.org/10.1016/j.enpol.2018.12.049
8. Gas Malaysia Berhad (2018) 2018 Annual report: embracing challenges and standing tall. Retrieved from https://www.gasmalaysia.com/index.php/investor-relations/annual-report
9. Seong CK, Abdullah M, Bin (1997) Peninsular gas utilisation project: planning and challenges to meet customers demand from the perspective of National Oil Company. In: SPE Asia pacific oil and gas conference. https://doi.org/10.2118/38074-MS
10. Aromada SA, Kvamme B (2019) Impacts of CO2 and H2S on the risk of hydrate formation during pipeline transport of natural gas. Front Chem Sci Eng 13:616–627. https://doi.org/10.1007/s11705-019-1795-2
11. Kvamme B, Kuznetsova T, Bauman JM, Sjöblom S, Avinash Kulkarni A (2016) Hydrate formation during transport of natural gas containing water and impurities. J Chem Eng Data 61(2):936–949. https://doi.org/10.1021/acs.jced.5b00787
12. Armenta M, Wojtanowicz A (2002) Severity of water coning in gas wells. In: SPE gas technology symposium, 737–746. https://doi.org/10.2523/75720-ms
13. Okereke NU, Edet PE, Baba YD et al (2019) An assessment of hydrates inhibition in deepwater production systems using low-dosage hydrate inhibitor and monoethylene glycol. J Petrol Explor Prod Technol. https://doi.org/10.1007/s13202-019-00812-4
14. Zaitoun A, Kohler N, Bossie-Codreanu D, Denys K (1999) Water shutoff by relative permeability modifiers: lessons from several field applications. In: SPE Annual technical conference and exhibition. https://doi.org/10.2523/56740-ms
15. Le Corre JM, Hervieu E, Ishii M, Delhaye JM (2003) Benchmarking and improvements of measurement techniques for local-time-averaged two-phase flow parameters. Exp Fluids. https://doi.org/10.1007/s00348-003-0697-7
16. Mandhane JM, Gregory GA, Aziz K (1974) A flow pattern map for gas-liquid flow in horizontal pipes. Int J Multiph Flow 1:537–553. https://doi.org/10.1016/0301-9322(74)90006-8
17. Chen IY, Yang KS, Chang YJ, Wang CC (2001) Two-phase pressure drop of air-water and R-410A in small horizontal tubes. Int J Multiph Flow 27(7):1293–1299. https://doi.org/10.1016/S0301-9322(01)00004-0
18. Kumar K, Thaker JP, Banerjee J (2013) Experimental investigations on two-phase flow phenomena in horizontal pipe. In: 40th National conference on fluid mechanics and fluid power. Himachal Pradesh, India
19. Ban S, Pao W, Nasif MS (2018) Numerical simulation of two-phase flow regime in horizontal pipeline and its validation. Int J Numer Meth Heat Fluid Flow 28(6):1279–1314. https://doi.org/10.1108/HFF-05-2017-0195
20. Hewitt G (1974) The flow of complex mixtures in pipes. J Fluid Mech 65(4):825–827. https://doi.org/10.1017/S0022112074211674
21. Kabiri-Samani AR, Borghei SM, Saidi MH (2007) Fluctuation of air-water two-phase flow in horizontal and inclined water pipelines. J Fluids Eng 129:1–14. https://doi.org/10.1115/1.2375134
22. Mukhaimer A, Al-Sarkhi A, El Nakla M, Ahmed WH, Al-Hadhrami L (2015) Effect of water salinity on flow pattern and pressure drop in oil-water flow. J Pet Sci Eng 128:145–149. https://doi.org/10.1016/j.petrol.2015.02.012
23. Besagni G, Inzoli F (2017) The effect of electrolyte concentration on counter-current gas–liquid bubble column fluid dynamics: gas holdup, flow regime transition and bubble size distributions. Chem Eng Res Des 118:170–193. https://doi.org/10.1016/j.cherd.2016.12.012
24. Xu Y, Fang X, Su X, Zhou Z, Chen W (2012) Evaluation of frictional pressure drop correlations for two-phase flow in pipes. Nucl Eng Des 253:86–97. https://doi.org/10.1016/j.nucengdes.2012.08.007

25. Haydary J (2019) Chemical process design and simulation: ASPEN plus and Aspen Hysys applications. American Institute of Chemical Engineers, Hoboken
26. Kawahara A, Yonemoto Y, Arakaki Y (2020) Pressure drop for gas and polymer aqueous solution two-phase flows in horizontal circular microchannel. Flow Turbul Combust. https://doi.org/10.1007/s10494-020-00127-z
27. Maher D, Hana A, Habib S (2020) New correlations for two phase flow pressure drop in homogeneous flows model. Therm Eng 67(2):92–105. https://doi.org/10.1134/S0040601520020032
28. Awad MM (2012) A simple two-phase frictional multiplier calculation method. In an overview of heat transfer phenomena sometimes, (Vol. 1). https://doi.org/10.5772/76201
29. Shannak BA (2008) Frictional pressure drop of gas liquid two-phase flow in pipes. Nucl Eng Des 238(12):3277–3284. https://doi.org/10.1016/j.nucengdes.2008.08.015
30. Kyi KK, Hashim H (2012) Fresh water conundrum in oil and gas reservoirs of Malaysia. Soc Pet Eng. https://doi.org/10.2118/158003-MS
31. Oddie G, Shi H, Durlofsky LJ, Aziz K, Pfeffer B, Holmes JA (2003) Experimental study of two and three phase flows in large diameter inclined pipes. Int J Multiph Flow 29(4):527–558. https://doi.org/10.1016/S0301-9322(03)00015-6
32. Donnelly GF, Spedding PL, McBride WJ (1995) Prediction of two and three phase flow in the horizontal configuration. In: Offshore technology conference, pp. 18–23. http://doi.org/10.4043/7743-MS
33. Woods GS, Spedding PL, Watterson JK, Raghunathan RS (1998) Three- phase oil/water/air vertical flow. Inst Chem Eng 76(July):571–584. https://doi.org/10.1205/026387698525252
34. Shi H, Holmes JA, Diaz LR, Durlofsky LJ, Aziz K (2004) Drift-flux parameters for three-phase steady-state flow in wellbores. SPE J 10(2):130–137. https://doi.org/10.2118/89836-PA
35. Spedding PL, Donnelly GF, Cole JS (2005) Three phase oil-water-gas horizontal co-current flow. Chem Eng Res Des 83(4):401–411. https://doi.org/10.1205/cherd.02154
36. Dong H, Zhang H, Sarica C (2009) Experimental study of low concentration sand transport in low liquid loading water-air flow in horizontal pipes. Multiph Prod Technol 4:17–27
37. Wang W, Gong J, Angeli P (2011) Investigation on heavy crude-water two phase flow and related flow characteristics. Int J Multiph Flow 37(9):1156–1164. https://doi.org/10.1016/j.ijmultiphaseflow.2011.05.011
38. Karami H, Torres CF, Pereyra E, Sarica C (2015) Experimental investigation of three-phase low liquid loading flow. In: SPE annual technical conference and exhibition (Vol. SPE 174926 MS). Houston, Texas, USA
39. Franca F, Lahey RT (1992) The use of drift-flux techniques for the analysis of horizontal two-phase flows. Int J Multiph Flow 18(6):787–801. https://doi.org/10.1016/0301-9322(92)90059-P
40. Wong TN, Yau YK (1997) Flow patterns in two-phase air-water flow. Int Commun Heat Mass Transf 24(1):111–118. https://doi.org/10.1016/S0735-1933(96)00110-8
41. Kim D, Ghajar AJ (2002) Heat transfer measurements and correlations for air-water flow of different flow patterns in a horizontal pipe. Exp Therm Fluid Sci 25(8):659–676. https://doi.org/10.1016/S0894-1777(01)00120-0
42. Zhang HQ, Wang Q, Sarica C, Brill JP (2003) Unified model for gas-liquid pipe flow via slug dynamics - part 1: model development. J Energy Res Technol 125(4):266–273. https://doi.org/10.1115/1.1615246
43. Fan Y (2005) An Investigation of low liquid loading gas-liquid stratified flow in near-horizontal pipes, PhD Thesis, The University of Tulsa, Tulsa, USA
44. Saisorn S, Wongwises S (2008) Flow pattern, void fraction and pressure drop of two-phase air-water flow in a horizontal circular micro-channel. Exp Therm Fluid Sci 32(3):748–760. https://doi.org/10.1016/j.expthermflusci.2007.09.005
45. Amaya-Gomez R, López J, Pineda H, Urbano-Caguasango D, Pinilla J, Ratkovich N, Muñoz F (2019) Probabilistic approach of a flow pattern map for horizontal, vertical, and inclined pipes. Oil Gas Sci Technol 74:67. https://doi.org/10.2516/ogst/2019034
46. Wang Y, Chang Y, Liu Z, Zhao X, Guo L (2020) Experimental and theoretical study of interface characteristics of gas–liquid stratified flow in horizontal pipe at high pressure. Flow Turbul Combust. https://doi.org/10.1007/s10494-020-00116-2
47. Garbai., R. & Sánta., L. (2012). Flow pattern map for in tube evaporation and condensation. In: 4th International symspsium on exploitation of renewable energy sources. Subotica, Serbia
48. Kee KE, Babic M, Richter S, Paolinelli L, Li W, Nesic S (2015) Flow patterns and water wetting in gas-oil-water three-phase flow - a flow loop study. In: Corrosion conferences and Expo. https://doi.org/NACE-2014-4068
49. Soedarmo A, Fan Y, Pereyra E, Sarica C (2018) A unit cell model for gas-liquid pseudo-slug flow in pipes. J Nat Gas Sci Eng 60:125–143. https://doi.org/10.1016/j.jngse.2018.10.006
50. Yang H, Zhao TS, Cheng P (2004) Gas-liquid two-phase flow patterns in a miniature square channel with a gas permeable sidewall. Int J Heat Mass Transf 47:5725–5739. https://doi.org/10.1016/j.ijheatmasstransfer.2004.07.025
51. Kesana NR, Parsi M, Vieira RE, Azzopardi B, Schleicher E, McLaury BS, Shirazi SA, Hampel U (2017) Visualization of gas-liquid multiphase pseudo-slug flow using wire-mesh sensor. J Nat Gas Sci Eng 46:477–490. https://doi.org/10.1016/j.jngse.2017.08.010
52. Al-Naser M, Elshafei M, Al-Sarkhi A (2015) Two-phase flow regimes identification using artificial neural network with nonlinear normalization. In: 2nd International conference on fluid flow, heat and mass transfer. Ontario, Canada: Avestia Publisher
53. Anumbe NC (2018) Scholar commons experimental investigation of two-phase (gas/liquid) flow in intermediate sized, horizontal and inclined Pipes, PhD Thesis, University of South Carolina, USA. Retrieved from https://scholarcommons.sc.edu/etd
54. Yusuf N, Al-Wahaibi Y, Al-Wahaibi T, Al-Ajmi A, Olawale AS, Mohammed IA (2012) Effect of oil viscosity on the flow structure and pressure gradient in horizontal oil-water flow. Chem Eng Res Des 90(8):1019–1030. https://doi.org/10.1016/j.cherd.2011.11.013
55. Wang Y (2018) A study of two-phase flow regime and pressure drop in vertical pipe. Master Thesis, University of North Dakota, USA. https://doi.org/10.1360/zd-2013-43-6-1064
56. Kawahara A, Chung PY, Kawaji M (2002) Investigation of two-phase flow pattern, void fraction and pressure drop in a microchannel. Int J Multiph Flow 28(9):1411–1435. https://doi.org/10.1016/S0301-9322(02)00037-X
57. Al-Wahaibi T, Smith M, Angeli P (2007) Effect of drag-reducing polymers on horizontal oil-water flows. J Pet Sci Eng 57(3–4):334–346. https://doi.org/10.1016/j.petrol.2006.11.002